Cell Cycle 11:10, 1918-1928; May 15, 2012; © 2012 Landes Bioscience

The DNA damage checkpoint protein ATM promotes hepatocellular apoptosis and fibrosis in a mouse model of non-alcoholic fatty liver disease

Erin K. Daugherity,[1,2] Gabriel Balmus,[2] Ahmed Al Saei,[2] Elizabeth S. Moore,[2] Delbert Abi Abdallah,[3] Arlin B. Rogers,[4] Robert S. Weiss[2,†,*] and Kirk J. Maurer[1,2,†,*]

[1]Center for Animal Resources and Education; Cornell University; Ithaca, NY USA; [2]Department of Biomedical Sciences; Cornell University; Ithaca, NY USA; [3]Department of Microbiology and Immunology; Cornell University; Ithaca, NY USA; [4]Department of Pathology and Laboratory Medicine; University of North Carolina; Chapel Hill, NC USA

[†]These authors contributed equally to this work.

Key words: nonalcoholic fatty liver disease, oxidative stress, ATM, steatoapoptosis, hepatic fibrosis

Abbreviations: NAFLD, nonalcoholic fatty liver disease; NASH, nonalcoholic steatohepatitis; HCC, hepatocellular carcinoma; FFA, free fatty acids; ROS, reactive oxygen species; ATM, ataxia telangiectasia mutated; DSB, double strand DNA breaks; A-T, ataxia telangiectasia; SD, standard diet; HFD, high-fat diet; IR, ionizing radiation; PUMA, p53 upregulated modulator of apoptosis; TUNEL, terminal deoxynucleotidyl transferase-mediated deoxyuridine triphosphate nick-end labeling; 8-OHG, 8-hydroxyguanosine; DHR, dihydrorhodamine 123

Steatoapoptosis is a hallmark of non-alcoholic fatty liver disease (NAFLD) and is an important factor in liver disease progression. We hypothesized that increased reactive oxygen species resulting from excess dietary fat contribute to liver disease by causing DNA damage and apoptotic cell death and tested this by investigating the effects of feeding mice high-fat or standard diets for 8 weeks. High-fat diet feeding resulted in increased hepatic H_2O_2, superoxide production and expression of oxidative stress response genes, confirming that the high-fat diet induced hepatic oxidative stress. High-fat diet feeding also increased hepatic steatosis, hepatitis and DNA damage as exemplified by an increase in the percentage of 8-hydroxyguanosine (8-OHG)-positive hepatocytes in high-fat diet-fed mice. Consistent with reports that the DNA damage checkpoint kinase ataxia telangiectasia mutated (ATM) is activated by oxidative stress, ATM phosphorylation was induced in the livers of wild-type mice following high-fat diet feeding. We therefore examined the effects of high-fat diet feeding in *Atm*-deficient mice. The prevalence of apoptosis and expression of the pro-apoptotic factor PUMA were significantly reduced in *Atm*-deficient mice fed the high-fat diet when compared with wild-type controls. Furthermore, high-fat diet-fed $Atm^{-/-}$ mice had significantly less hepatic fibrosis than $Atm^{+/+}$ or $Atm^{+/-}$ mice fed the same diet. Together, these data demonstrate a prominent role for the ATM pathway in the response to hepatic fat accumulation and link ATM activation to fatty liver-induced steatoapoptosis and fibrosis, key features of NAFLD progression.

Introduction

Nonalcoholic fatty liver disease (NAFLD) is an emerging health epidemic with a poorly understood pathogenesis.[1] NAFLD comprises a spectrum of hepatic lesions ranging from steatosis with deposition of triglycerides within hepatocytes to the more aggressive nonalcoholic steatohepatitis (NASH), which includes hepatitis and fibrosis.[1,2] Fatty liver disease is highly prevalent in the US, with an estimated 30% of the population possessing NAFLD and 6% suffering from NASH. These numbers rise to 90% and 30% respectively when obese populations are examined.[3] NASH-induced complications are severe, and approximately one-third of NASH patients develop cirrhosis and may progress to hepatocellular carcinoma (HCC) or liver failure.[1,2,4] There is a clear link between dietary fat consumption and fatty liver disease; however, the factors that promote the progression of NAFLD to NASH and its associated complications currently are not well understood.[2,5-7]

During NAFLD/NASH, an excessive amount of nonesterified free fatty acids (FFAs) overwhelm the ability of the liver to convert FFAs to triglycerides, resulting in apoptotic cell death, a process known as steato- or lipoapoptosis.[8,9] In both humans and animal models, hepatocyte apoptosis correlates with NASH severity and fibrosis stage, suggesting that steatoapoptosis plays

*Correspondence to: Robert S. Weiss and Kirk J. Maurer; Email: rsw26@cornell.edu and km429@cornell.edu
Submitted: 01/12/12; Revised: 04/02/12; Accepted: 04/03/12
http://dx.doi.org/10.4161/cc.20259

a causative role in disease progression.[9-13] The exact mechanisms and cellular pathways linking hepatic lipid accumulation to steatoapoptosis and the progression of NAFLD/NASH remain largely unknown. However, oxidative stress may have a central role, as oxidative metabolism is increased in NAFLD patients,[14] and recent studies indicate that saturated FFAs induce apoptosis through the generation of reactive oxygen species (ROS).[13]

Eukaryotic cells protect genomic integrity in part through checkpoint mechanisms, including a pathway centered on the protein kinase ataxia telangiectasia mutated (ATM), which is activated by double-strand DNA breaks (DSB). Once activated, ATM phosphorylates intermediary protein substrates, including CHK2, p53 and H2AX, leading to cell cycle arrest and DNA repair or apoptosis.[15] Failure to activate ATM after DNA damage leads to defective cell cycle control and impaired DNA repair. In humans, ATM deficiency results in the genomic instability syndrome ataxia telangiectasia (A-T). A-T patients cannot respond to DSB properly, resulting in a variety of deleterious phenotypes, including cerebellar ataxia, immunodeficiency, premature aging, sterility, chromosomal instability, shortened lifespan and cancer predisposition.[15] ATM is also implicated in metabolic disease, characterized by a variety of conditions, including insulin resistance, glucose intolerance, elevated serum cholesterol and lipid levels and atherosclerosis.[16,17] Importantly, ATM can be directly activated by ROS independent of DSBs, and ROS-induced ATM signaling is associated with phosphorylation of only a subset of ATM targets, including p53 and CHK2 but not H2AX.[17,18] Further, cultured *Atm*-deficient cells are more sensitive to oxidative stress.[19] Hepatocytes with excess fat are exceptionally vulnerable to oxidative stress and DNA damage,[4,14,20] but the potential role of ATM in this process is unknown.

Due to the increasing prevalence of NAFLD/NASH and the clear connection to complications including HCC, the overall objective of this study was to establish and characterize an inducible animal model capable of mechanistically evaluating the interaction between hepatic fat accumulation, DNA damage, oxidative stress and NAFLD/NASH disease progression. Our results demonstrate that lipid-laden hepatocytes experience increased oxidative stress and undergo ATM-dependent steatoapoptosis, which occurs independently of detectable H2AX phosphorylation. These findings provide strong evidence that an ATM-mediated DNA damage response contributes to NAFLD progression by promoting apoptosis and fibrosis in the liver.

Results

Hepatic oxidative stress is promoted by high-fat diet feeding. Feeding mice a high-fat diet with cholesterol and cholic acid leads to increased expression of oxidative stress-related genes.[21] We directly measured oxidative stress associated with excessive fat consumption by harvesting hepatocytes from mice fed either a standard diet (SD) or a high-fat diet (HFD) for 8 weeks and performing Amplex Red staining to detect H_2O_2 and dihydrorhodamine (DHR) staining to detect superoxide species. Hepatocytes from mice fed the HFD (n = 4) showed significantly elevated levels of H_2O_2 compared with SD-fed mice (n = 3) (**Fig. 1A**; *p < 0.05). Superoxide levels, as measured by DHR staining, were also significantly increased in hepatocytes from HFD-fed mice as compared with those from SD-fed animals (**Fig. 1B and C**; *p = 0.01). Quantitative PCR analysis of the NADPH oxidase *p22phox* gene, which plays a central role in superoxide production,[21] additionally was performed. Consistent with the H_2O_2 and superoxide quantification, there were significant increases in *p22phox* expression in livers from HFD-fed mice compared with those from mice fed SD (**Fig. 1D**; *p = 0.002). These data indicate that HFD feeding causes increased oxidative stress in hepatocytes.

High-fat diet feeding induces hepatomegaly, steatohepatitis and ATM activation and promotes hepatic fibrosis in an *Atm*-dependent manner. ATM activation plays an important role in the cellular response to ROS, and A-T patients display increased sensitivity to oxidative stress.[18,19,22] We therefore assessed ATM pathway activation in mice following HFD feeding via immunofluorescent staining of liver sections using an antibody that detects phosphorylated, active ATM (pS1987 of mouse ATM, corresponding to pS1981 of human ATM).[23] Hepatocytes from Atm^+ ($Atm^{+/+}$ and $Atm^{+/-}$) HFD-fed mice displayed both nuclear and cytoplasmic foci containing p-ATM, while hepatocytes from Atm^+ SD-fed mice did not, confirming hepatic ATM activation in the Atm^+ HFD-fed group (**Fig. 2A**). The majority of the foci appeared to be localized to the periphery of the nucleus. The detection of HFD-induced ATM phosphorylation was specific, as no staining was observed in $Atm^{-/-}$ hepatocytes from mice fed either diet. We next tested the ability of *Atm*-deficient mice to respond to HFD feeding. Livers were examined grossly and microscopically after 8 weeks of feeding SD or HFD to determine if HFD feeding induced hepatic changes consistent with NAFLD. For all measures described below, we observed no significant differences between $Atm^{+/+}$ and $Atm^{+/-}$ mice and, therefore, in most cases present combined data for these genotypes under the label Atm^+. Irrespective of *Atm* status, there was 100% prevalence of fatty liver development in mice fed the HFD (n = 22), whereas all mice fed the SD (n = 23) had grossly normal livers (**Fig. 2B**). Mice fed the HFD also had marked increases in liver weight (**Fig. 2C**; *p < 0.0001) but not in total body weight (**Fig. 2C and D**) compared with mice fed the SD, indicating that the HFD induced hepatic fat accumulation independent of obesity. Consistent with previous reports in references 24–26, $Atm^{-/-}$ mice had slightly lower body weights compared with Atm^+ mice regardless of diet (**Fig. 2D**). Upon both H&E and Oil-red-O staining, hepatocytes from HFD-fed $Atm^{+/+}$ and $Atm^{-/-}$ mice displayed marked cellular hypertrophy and both microvesicular and macrovesicular steatosis (**Fig. 3A**). In contrast, there was no abnormal hepatic fat accumulation in mice fed the SD. Further, mice fed the HFD had significantly higher fatty liver scores compared with SD-fed controls irrespective of *Atm* genotype (**Fig. 3B**,*p < 0.0001). These data demonstrate that 8 weeks of HFD feeding produced marked hepatic steatosis consistent with NAFLD in both *Atm*-expressing and *Atm*-deficient mice.

Additional hepatic phenotypes resulting from 8 weeks of HFD feeding were evaluated based on H&E staining and pico-sirius

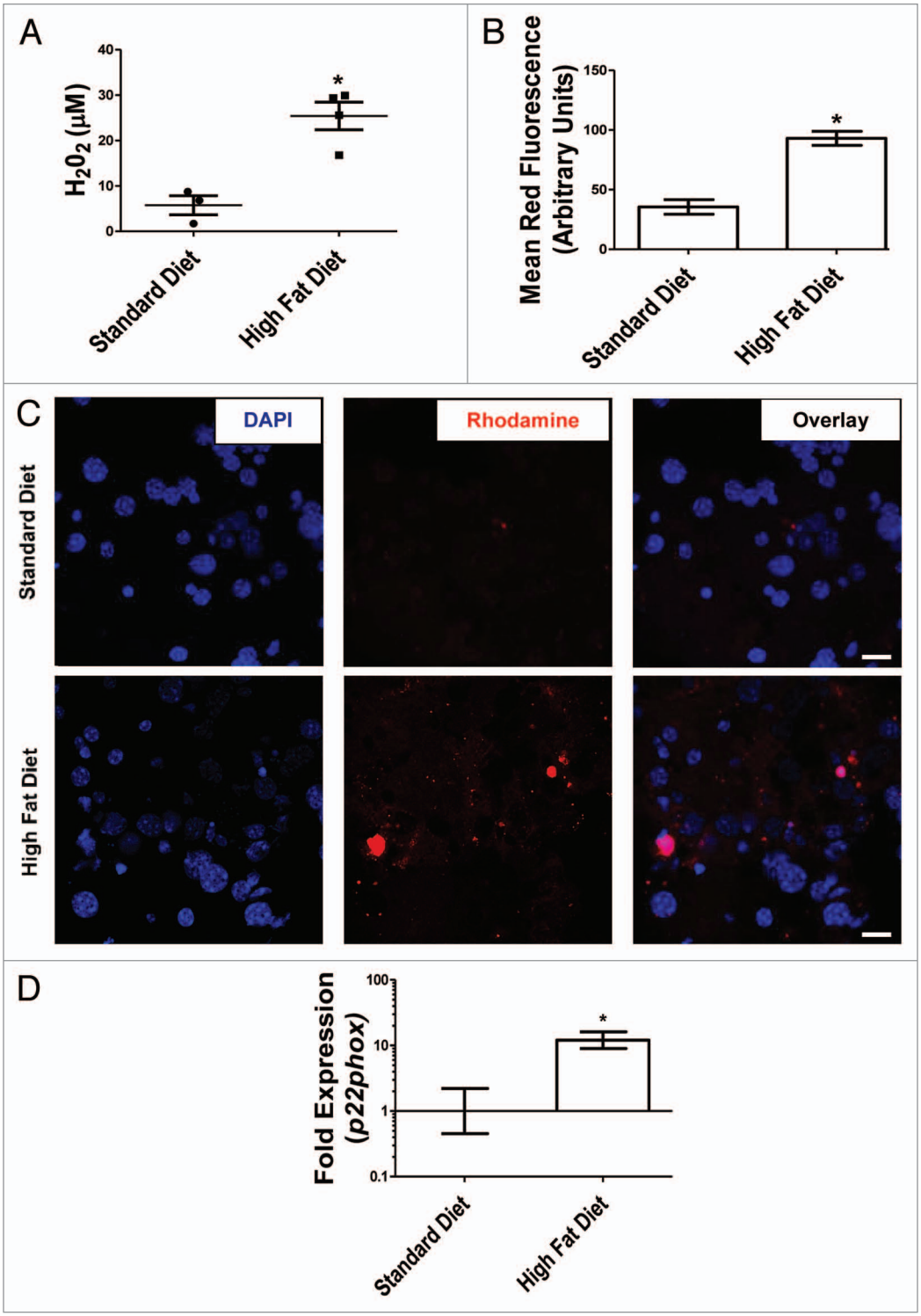

Figure 1. High-fat diet feeding induces hepatic oxidative stress. Mice were fed SD or HFD for 8 weeks. Hepatocytes were then harvested and analyzed for (A) hydrogen peroxide production (Amplex-Red assay) or (B and C) the presence of superoxide (dihydrorhodamine assay). (A) Comparison of hydrogen peroxide levels showed that hepatocytes from mice fed the HFD (n = 4) produced significantly more hydrogen peroxide compared with mice fed the SD (n = 3) (*$p < 0.05$, Student t-test). Scatter dot plot results are expressed as mean ± SEM. (B) Comparison of the mean red fluorescence of DHR stained livers from SD and HFD fed groups (n = 3 for both groups) showed that mice fed the HFD displayed significantly more red fluorescence than the SD-fed mice (*$p = 0.01$, Student t-test). Results are expressed as mean ± SEM on a scale of 0–250. (C) Dihydrorhodamine (DHR) fluorescent staining of hepatocytes harvested from mice fed the SD (top row) and HFD (bottom row). Scale bars represent 5 μm. (D) Quantitative PCR analysis of the NADH/NADPH oxidase *p22 phox* gene from mice fed SD or HFD demonstrated significant increases in the HFD group compared with the SD group (*$p = 0.002$, Student t-test). Gene expression was normalized to *Gapdh* expression and was compared by the $\Delta\Delta C_T$ method.

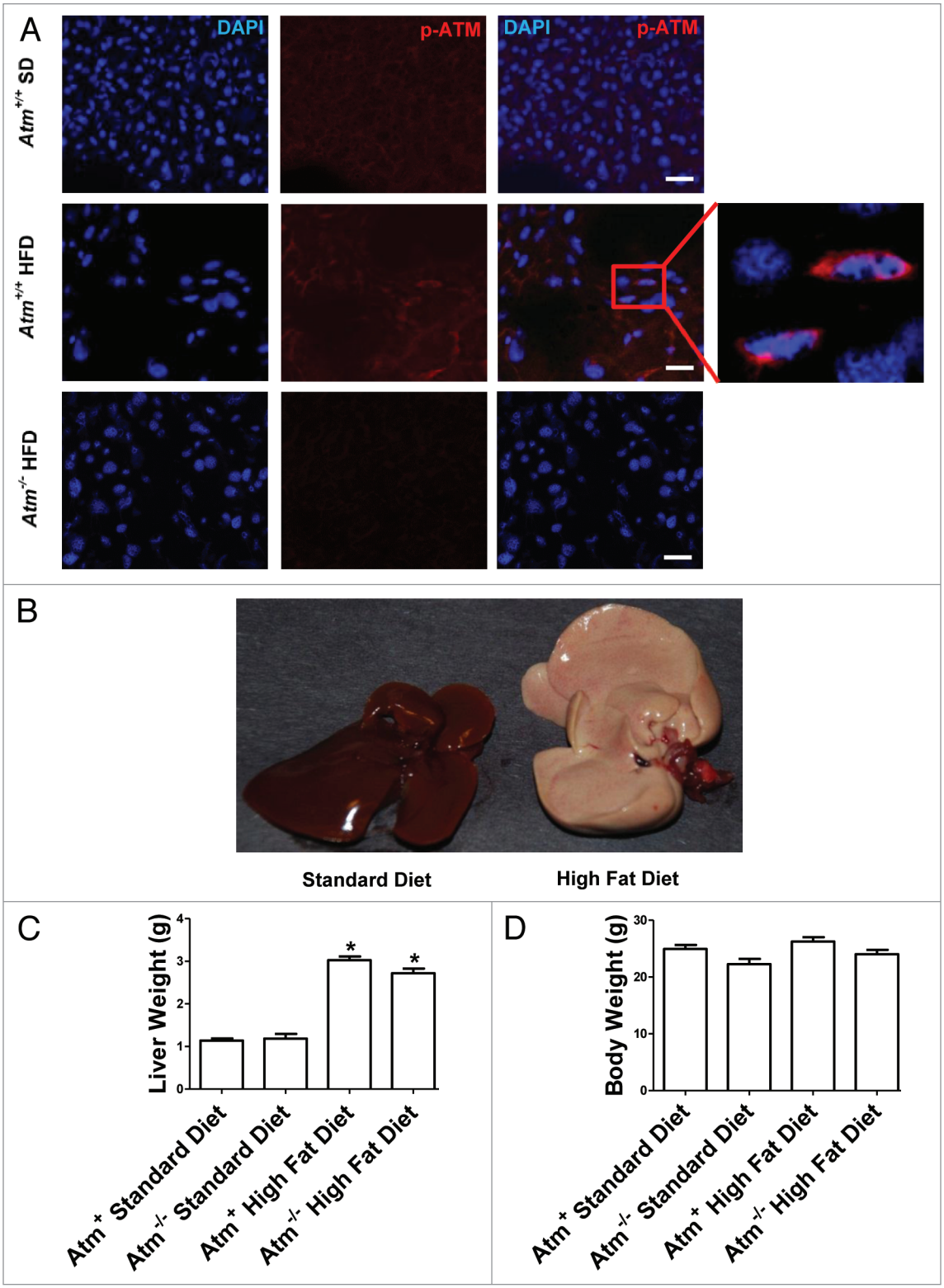

Figure 2. High-fat diet feeding induces grossly evident fatty liver without fat accumulation in other tissues. *Atm*$^{+}$ and *Atm*$^{-/-}$ mice were fed SD or HFD for 8 weeks. Liver weight, body weight and liver appearance were evaluated post euthanasia. Hepatocytes were then harvested and analyzed by immunofluorescence. (A) Frozen sections of livers from *Atm*$^{+/+}$ mice fed SD or HFD and *Atm*$^{-/-}$ mice fed the HFD were labeled with anti-phospho-ATM (p-ATM) antibody and examined by confocal microscopy. Blue fluorescence signals represent DAPI stained nuclei and positive p-ATM foci fluoresce red. Scale bars represent 2.5 μm. (B) Representative images of liver from SD and HFD groups at the time of euthanasia. Scale bars represent 0.5 cm. (C) Comparison of liver weights and (D) total body weights of mice of the indicated genotypes after 8 weeks of HFD or SD feeding showed that mice fed the HFD had marked increases in liver weight compared with mice fed the SD (*$p < 0.0001$, Student t-test). Results are expressed as mean ± SEM.

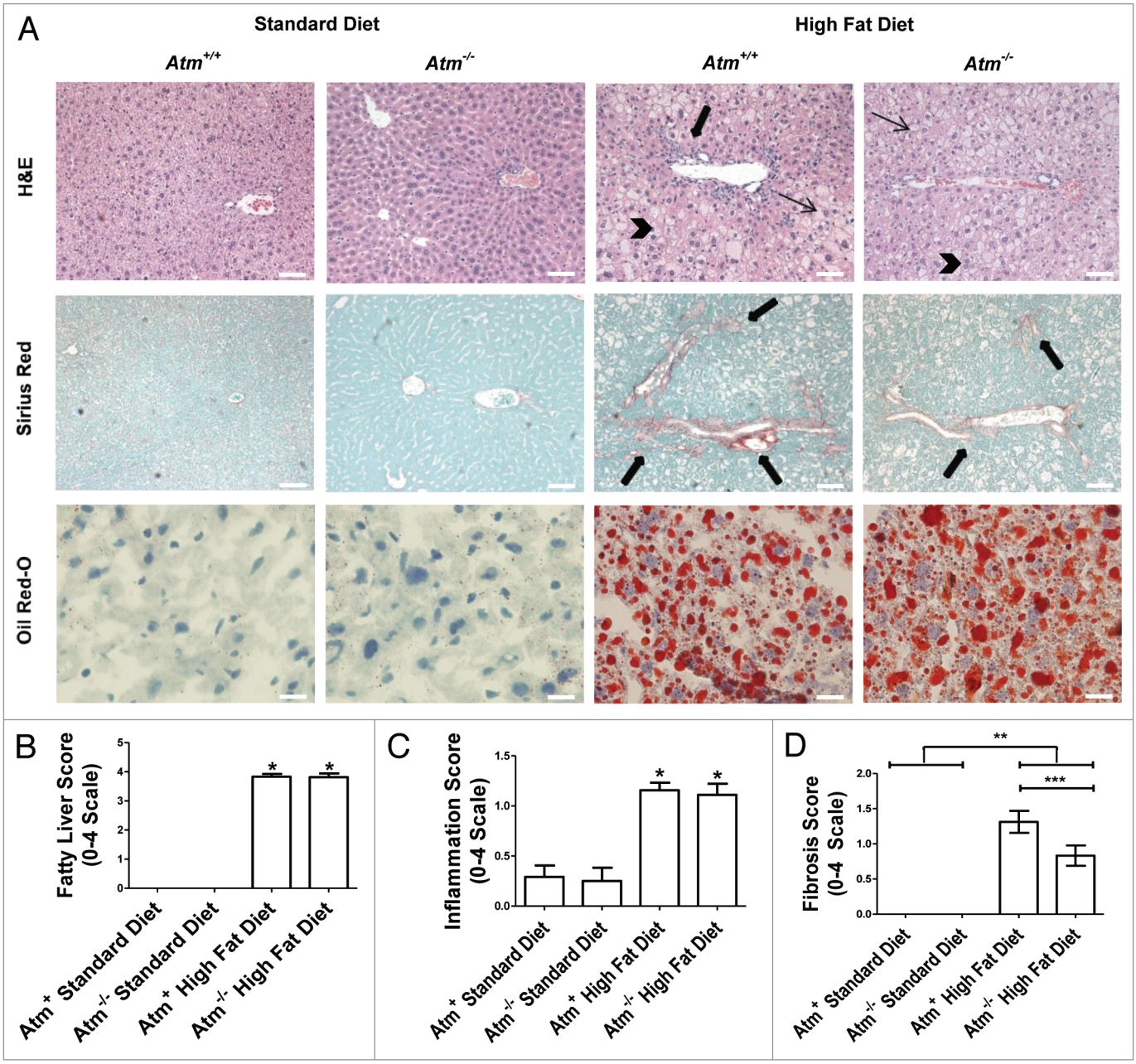

Figure 3. High-fat diet feeding induces hepatic steatosis and hepatitis regardless of *Atm* status, but leads to more fibrosis in *Atm*$^{+}$ livers. H&E (A, first row, scale bars represent 20 μm), Sirius red (A, second row, scale bars represent 20 μm) and Oil-Red-O (A, third row, scale bars represent 10 μm) sections from mice fed SD (n = 20) or HFD (n = 25) for 8 weeks were scored blindly on a scale of 0–4 for fat accumulation (B), inflammation (C) and fibrosis (D). Results are expressed as mean ± SEM. Statistical values were obtained using Mann-Whitney-U test followed by Dunn's post test. Comparison of scores between HFD and SD-fed mice showed that regardless of *Atm* status, mice fed HFD had significantly higher fatty liver (B; *$p < 0.0001$), inflammation (C; *$p < 0.05$) and fibrosis (D; **$p < 0.05$) scores when compared with mice fed SD. Additionally, *Atm*$^{+}$ mice fed the HFD developed significantly higher fibrosis scores (D, ***$p < 0.05$) compared with *Atm*$^{-/-}$ mice. Differences in fibrosis were highlighted by fewer Sirius red-positive foci in *Atm*$^{-/-}$ mice (A, second row, arrows). H&E staining of livers from SD fed *Atm*$^{+}$ and *Atm*$^{-/-}$ mice revealed histologically normal liver, while mice of both genotypes, when fed the HFD, displayed cellular hypertrophy and accumulation of microvesicular (arrow head) and macrovesicular (thin arrows) steatosis, and portal inflammation (thick arrows). Mice fed the SD did not develop inflammation. Oil Red-O staining confirmed the presence of marked lipid accumulation in HFD fed livers.

red staining for collagen. Livers from both *Atm*$^{+}$ and *Atm*$^{-/-}$ mice fed the HFD demonstrated moderate, predominantly peri-portal, mixed inflammatory cell infiltrates (**Fig. 3A**). In contrast, there were no hepatic inflammatory lesions in mice fed the SD. Further, all mice fed the HFD, regardless of genotype, had significantly higher inflammation (**Fig. 3C**, *$p < 0.05$) and fibrosis (**Fig. 3D**, **$p < 0.05$) scores when compared with mice fed the SD. Notably, *Atm*$^{+}$ HFD-fed mice developed significantly more

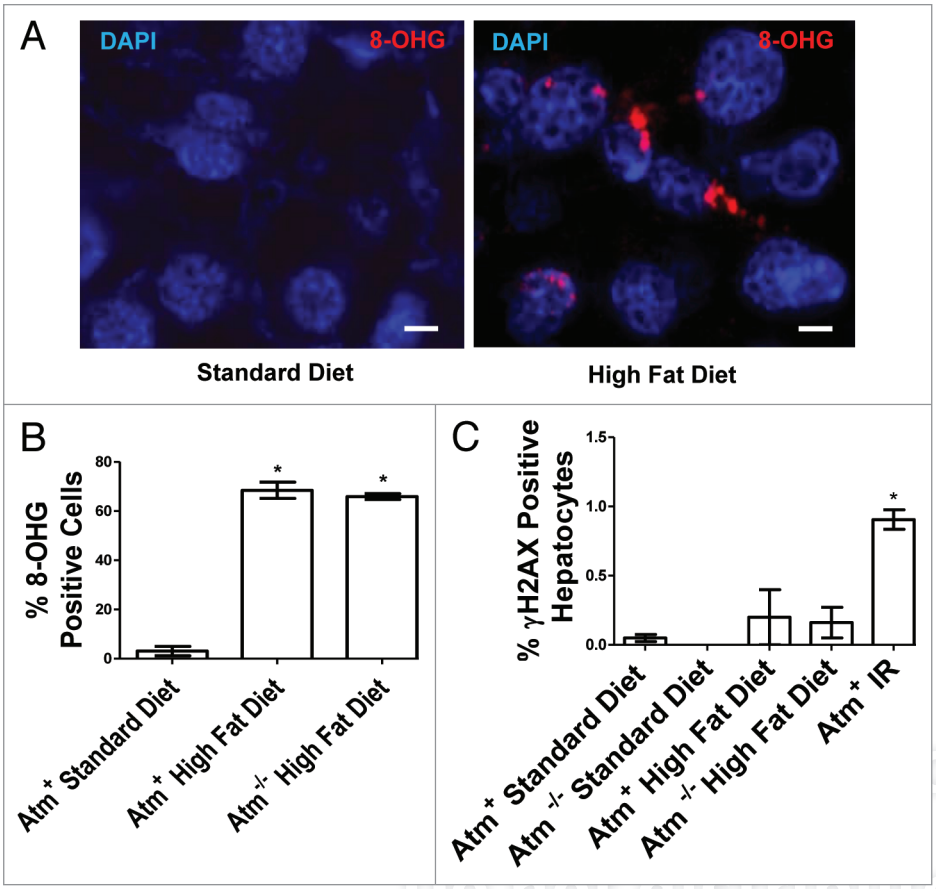

Figure 4. High-fat diet feeding increases hepatic nucleic acid damage but does not induce detectable phosphorylation of histone H2AX. (A) Frozen sections of livers from mice fed SD (left) or the HFD (right) were labeled with anti-8-hydroxyguanosine (8-OHG) antibody and examined by confocal microscopy. Blue fluorescence signals represent DAPI stained nuclei and positive 8-OHG foci fluoresce red. Scale bars represent 2.5 μm. (B) Quantitation of the experiment described in (A) highlights that there were significantly more 8-OGH positive nuclei per 80x field in the *Atm*$^{+}$ and *Atm*$^{-/-}$ groups fed the HFD than in the *Atm*$^{+}$ group fed the SD (*p = 0.001, Student t-test) (n = 3 in each group). Results are expressed as mean ± SEM. The percentage of 8-OHG positive nuclei out of total DAPI-positive nuclei was calculated over three 80x fields. (C) Immunohistochemistry was performed to identify phosphorylated histone H2AX in liver sections from HFD and SD-fed mice of the indicated genotypes (n = 3/group) and revealed that there was minimal staining in these groups, while there was significantly more staining detected in *Atm*$^{+}$ livers treated with 10 Gy IR regardless of genotype (*p < 0.0001, Student t-test). Data on graph represent mean ± SEM.

fibrosis than *Atm*$^{-/-}$ mice (**Fig. 3D**, ***p < 0.05). Differences in fibrosis development were highlighted by fewer and smaller picosirius red-positive foci in the livers of *Atm*$^{-/-}$ mice as compared with those of *Atm*$^{+}$ mice (**Fig. 3A**). These data demonstrate that 8 weeks of HFD feeding produces marked steatohepatitis regardless of *Atm* status, and that subsequent fibrosis is dependent, at least in part, on ATM.

High-fat diet feeding induces oxidative nucleic acid damage but limited histone H2AX phosphorylation. To understand the basis for the effects of *Atm* deficiency on HFD-induced liver pathology, we evaluated whether *Atm* loss affects ROS levels in HFD-fed mice. To a similar extent as was observed in *Atm*$^{+}$ mice (**Fig. 1**), HFD feeding of *Atm*$^{-/-}$ mice caused increased H_2O_2 and superoxide accumulation relative to SD-fed mice (**Fig. S1**). Levels of 8-hydroxyguanosine (8-OHG), an oxidized nucleotide and marker of oxidative nucleic acid damage were then quantified to determine if the elevated oxidative stress in fatty livers resulted in hepatocyte DNA damage. There was minimal staining for 8-OHG in the SD group, while there were multiple 8-OHG-positive aggregates within the nuclei and cytoplasm of hepatocytes from HFD-fed mice (**Fig. 4A**). In some nuclei, 8-OHG appeared to be localized to the periphery of the nucleus. Quantification of 8-OHG-positive cells showed that there were significantly more positive cells in the *Atm*$^{+}$ and *Atm*$^{-/-}$ groups fed the HFD than in mice fed the SD (**Fig. 4B**; *p = 0.001). There was no significant difference between *Atm*$^{+}$ and *Atm*$^{-/-}$ HFD-fed groups. These findings indicate that the HFD causes oxidative nucleic acid damage in both *Atm*-expressing and *Atm*-deficient mice.

To determine the nature and extent of the DNA damage response induced by HFD feeding, we performed immunohistochemistry on liver sections from HFD- and SD-fed groups and quantified the levels of γH2AX, the phosphorylated form of histone H2AX which occurs in response to DNA DSBs.[27] In contrast to our earlier observations of HFD feeding-induced ATM phosphorylation (**Fig. 2A**), there was minimal positive staining for H2AX phosphorylation in hepatic nuclei from mice of all experimental groups (**Fig. 4C; Fig. S2**; *p < 0.0001). Importantly, significant increases in γH2AX staining were detected in liver sections from control mice treated with ionizing radiation. Overall, these data demonstrate that there is DNA damage in HFD fed hepatocytes without substantial phosphorylation of H2AX.

High-fat diet feeding increases *Atm*-dependent steatoapoptosis. One of the outcomes of ATM pathway activation is apoptosis,[15] and steatoapoptosis is important in fatty liver progression.[9,12,13] The induction of apoptosis by HFD feeding was evaluated by terminal uridine deoxynucleotidyl transferase dUTP nick end labeling (TUNEL) staining of liver sections (n = 5–10/group). TUNEL staining detects DNA fragmentation, a characteristic feature of apoptotic cells. HFD groups contained significantly more TUNEL-positive hepatocytes compared with SD groups, which exhibited minimal positive staining (**Fig. 5A**; **Fig. S3**; *p ≤ 0.0001). Notably, among the HFD-fed mice, *Atm*$^{+}$ hepatocytes underwent significantly more apoptosis than those

from *Atm*$^{-/-}$ mice (**Fig. 5A**; **p < 0.001). To dissect the molecular basis for this ATM-dependent apoptotic response to HFD feeding, we used quantitative PCR to measure the expression of the DNA damage-responsive, pro-apoptotic gene *Puma*.[28] HFD-fed *Atm*$^{+}$ mice (n = 12) had increased *Puma* expression when compared with all other groups, including HFD-fed *Atm*-deficient mice (n = 10–12/group), indicating that PUMA is induced after HFD feeding through a mechanism that requires ATM (**Fig. 5B**; *p < 0.01). HFD feeding similarly resulted in increased PUMA protein levels as measured by immunoblotting of livers from *Atm*$^{+}$ HFD-fed mice, and this induction of PUMA was greatly reduced in samples from *Atm*-deficient mice (**Fig. 5C**). Together, these data indicate that HFD feeding induces ATM-dependent upregulation of PUMA and hepatocyte apoptosis.

Discussion

NAFLD represents an array of hepatic lesions ranging from benign steatosis to hepatic inflammation and cirrhosis. Because of the increasing prevalence of this disease, a more thorough understanding of the factors involved in NAFLD progression is warranted. This study investigated the roles of ATM, a protein kinase involved in maintaining genomic stability, in a diet-induced model of NAFLD/NASH. Other models of NASH use genetic defects, chemical agents or nutrient depletion to induce steatohepatitis and hepatic fibrosis. Nutritional models, such as sucrose- and fructose-rich diets, cause only minimal hepatic steatosis and inflammation.[21] Conversely, the diet used in this study closely recreated the NAFLD phenotype of steatohepatitis and fibrosis by coupling high fat with cholesterol and cholic acid. Fat accumulation elsewhere in the body was not observed, presumably due to the fat source and the relatively short time period mice were fed the HFD.

Eight weeks of HFD feeding caused hepatic phenotypes in mice, consistent with NAFLD, including hepatic steatosis and oxidative stress indicated by elevated levels of ROS and increased expression of *p22phox*, a gene encoding a subunit of NADPH oxidase. Hepatic lipid accumulation is considered an initiating factor in NAFLD pathogenesis and renders hepatocytes susceptible to oxidative stress. High levels of oxidative stress correlate with increasing severity of liver disease in humans.[4] In this study, we showed that HFD-induced steatohepatitis and hepatic oxidative stress were present in both *Atm*$^{+}$ and *Atm*$^{-/-}$ mice, which recapitulates essential components of NAFLD/NASH and creates a hepatic environment ideal to study the effects of *Atm* loss on NAFLD progression.

Chronic liver injury results in fibrosis.[29,30] After 8 weeks of HFD feeding, *Atm*$^{+}$ mice exhibited more hepatic fibrosis than *Atm*$^{-/-}$ mice. Interestingly, the same trend was observed for hepatic apoptosis, with *Atm*$^{+}$ mice exhibiting more hepatocyte apoptosis than *Atm*$^{-/-}$ mice after chronic HFD feeding. This is consistent with data indicating that apoptosis contributes to fibrosis in NAFLD/NASH progression as well as with in vitro studies that suggest a direct link between hepatocyte apoptosis and fibrosis.[10,12,13,31] Although the precise mechanistic details have not been fully resolved, available data indicate that apoptosis and cell clearance stimulate quiescent hepatic stellate cells, triggering their transformation to a myofibroblast phenotype and subsequent extracellular matrix deposition.[11,32]

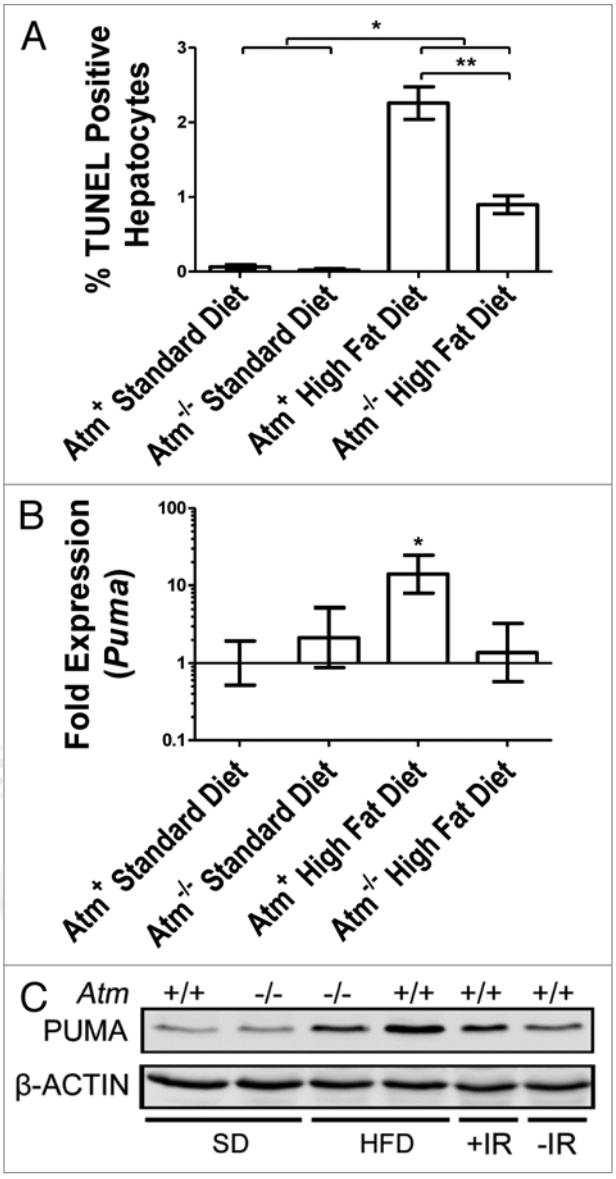

Figure 5. High-fat diet feeding induces *Atm*-dependent steatoapoptosis. (A) TUNEL staining to identify apoptotic cells in liver sections from mice of the indicated group (n = 5–10/group) was quantified and revealed that HFD groups, regardless of genotype, contained significantly more TUNEL-positive hepatocyte nuclei compared with the SD (*p < 0.0001, Student t-test). Comparison of TUNEL quantification from HFD-fed mice showed that hepatocytes from *Atm*$^{+}$ mice underwent significantly more apoptosis than those from *Atm*$^{-/-}$ mice (**p < 0.001). Data represent mean ± SEM. (B) Quantitative PCR analysis of the pro-apoptotic gene *Puma* from *Atm*$^{+}$ and *Atm*$^{-/-}$ mice fed either SD or HFD for 8 weeks demonstrated that the *Atm*$^{+}$ HFD mice (n = 12) had increased *Puma* expression when compared with all other groups (n = 10–12/group) (*p < 0.01, Student t-test). (C) Total protein lysates were prepared from frozen liver section after feeding SD or HFD and immunoblotted for PUMA. Liver lysates from untreated (-IR) or ionizing radiation treated (+IR, 2 h post-5 Gy) mice were used as negative and positive controls respectively. β-actin was used as a loading control.

Differences in fibrosis and steatoapoptosis between HFD-fed *Atm*$^{+}$ and *Atm*$^{-/-}$ mice correlated with expression levels of the pro-apoptotic gene *Puma* at both the mRNA and protein levels. Excessive ROS production, as seen in this model, may induce apoptosis via various pathways, including the intrinsic pathway of apoptosis, which involves PUMA signaling.[11,33] Recent studies identify PUMA as an important factor in hepatocyte steatoapoptosis, and PUMA inhibition or deficiency leads to decreased hepatic apoptosis.[33-36] Moreover, hepatic *Puma* expression is increased in NASH patients as compared with expression levels in NAFLD or healthy patients, implicating PUMA in fatty liver disease progression, likely through functions related to steatoapoptosis and fibrosis formation.[9,34] *Puma* activation relies primarily on the DNA damage-inducible transcription factor p53.[33] ATM is an upstream activator of p53, linking ATM to PUMA-mediated apoptosis in a manner consistent with the ATM-dependent upregulation of *Puma* expression in this model. We also evaluated components of the extrinsic pathway of apoptosis, including *Fas* and *Fas receptor*, via quantitative PCR. There were appreciable increases in *Fas receptor* expression between SD and HFD groups, but the levels were nearly identical between *Atm*$^{+}$ and *Atm*$^{-/-}$ HFD groups (**Fig. S4**). Further, there was no detectable expression of *Fas* ligand in any treatment group (data not shown). Although we cannot entirely rule out involvement of the extrinsic pathway of apoptosis in high-fat-mediated apoptotic cell death, it does not appear to account for differences observed in hepatocyte death between HFD fed *Atm*$^{+}$ and *Atm*$^{-/-}$ mice.

One of the most common causes of hepatic genomic instability is ROS-induced DNA damage.[37,38] In this study, chronic HFD feeding caused oxidative nucleic acid damage regardless of *Atm* status as evidenced by the similar percent of 8-OHG-positive cells in HFD-fed *Atm*$^{+}$ and *Atm*$^{-/-}$ mice. Interestingly, phosphorylation of histone H2AX, a marker of DNA DSBs, was not detectably induced in the HFD groups. γH2AX-positive hepatocytes were present in IR-treated control samples, demonstrating that the immunohistochemical assay for γH2AX was functional. Thus, hepatocytes are capable of phosphorylating H2AX but do not do so to a detectable level in response to HFD feeding. Studies show that ROS-induced ATM activation can occur in the absence of DNA DSBs, and this is associated with phosphorylation of only a subset of ATM targets that does not include H2AX.[17,18] Taken together, these data suggest that ATM-mediated fatty liver phenotypes may be the result of an oxidative stress response rather than the classical γH2AX associated signaling pathway. The observation of phospho-ATM in the cytoplasm of fat-laden hepatocytes provides further support for a ROS-mediated mechanism of ATM activation.[17] Within the nucleus, both 8-OHG and p-ATM seemed to be more abundant at the nuclear periphery. One hypothesis to explain the observed localization of 8-OHG is that the low permeability of reactive oxygen species limits their mobility through the nuclear membrane, thus creating the most extensive oxidative damage at the nuclear periphery.[39] The observed staining patterns also may relate to previous in vitro studies, demonstrating that oxidative damage preferentially occurs in heterochromatin, which is predominantly located in the nuclear periphery, and that ATM is critical in repairing this damage.[40]

NASH carries a risk of HCC formation. It is well established that apoptosis promotes hepatic fibrosis, and both are key risk factors for HCC development, with hepatic fibrosis and cirrhosis being present in 80–90% of patients with HCC.[30,41,42] In this study, steatoapoptosis and fibrosis were observed at highest levels in ATM-expressing HFD-fed mice, indicating that the ATM pathway promotes both during hepatic lipid accumulation. Although apoptosis is generally regarded as a tumor-suppressing mechanism that clears damaged cells at risk of undergoing malignant transformation, there also are several examples of tumor-promoting effects of apoptosis, including in HCC.[43] Here, the ultimate effect of reduced fibrosis and apoptosis on tumor development could not be determined, because *Atm*$^{-/-}$ mice develop thymic lymphoma at 3–4 mo of age,[24-26] preventing long-term evaluation of liver carcinogenesis. However, based upon the recognized influences of apoptosis and fibrosis during HCC development, it is reasonable to hypothesize that the observed *Atm*-dependent increases in these processes could promote hepatic carcinogenesis. Therefore, pharmacological inhibition of ATM may be beneficial to limit fibrosis formation and NAFLD progression.

In summary, our findings suggest that hepatic fat accumulation triggers oxidative stress and activation of an ATM-mediated DNA damage response, resulting in steatoapoptosis and hepatic fibrosis. Human trials have been inconclusive regarding effective therapy for NAFLD, including antioxidants, insulin sensitizers, weight loss or a combination of these modalities.[44,45] However, our data suggest that modulation of ROS levels and ATM activation may provide novel therapeutic targets to prevent the progression of NAFLD. The mouse model described here provides a system for further experimental evaluation of how candidate therapeutics, like the antioxidants NAC and Tempol, which suppress the ROS to which ATM responds,[46-48] impact fatty liver disease.

Materials and Methods

Animal husbandry. *Atm*-null mice were used on a FVB/N strain background.[25] *Atm*$^{+/-}$ mice were intercrossed, and progeny were divided into four study groups. In the first and second group, *Atm*$^{+}$ (*Atm*$^{+/+}$ and *Atm*$^{+/-}$) and *Atm*$^{-/-}$ mice were fed a standard diet (SD) (<0.05% cholesterol, 0% cholic acid, 5% triglyceride; 7012 Harlan Teklad LM-485 Mouse/Rat Sterilizable Diet), and in the third and fourth groups, *Atm*$^{+}$ and *Atm*$^{-/-}$ mice were fed a high-fat diet (HFD) (1.0% cholesterol, 0.5% cholic acid, 18% triglyceride; TD.880511, Harlan, Teklad Lab Animal Diets; "Paigen diet") for eight weeks. Initially, both sexes were assessed separately; however, no differences were seen between the sexes, and male and female data were combined (data not shown). Likewise, data from *Atm*$^{+/-}$ and *Atm*$^{+/+}$ mice were initially evaluated independently and combined when data indicated there were no differences between these groups. A subset of mice was whole-body irradiated with 10 Gy irradiation 8 h prior to tissue collection. Mice were housed under specific pathogen-free conditions in an

Association for the Assessment and Accreditation of Laboratory Animal Care International accredited facility. Mice received food and water ad libitum. All protocols were approved by the Cornell University Institutional Animal Care and Use Committee.

Tissue harvest and histopathology. After eight weeks of HFD or SD feeding, mice were euthanized with CO_2. The liver was removed aseptically and weighed. Approximately 30 mg of liver was flash frozen in both liquid N_2 and in Tissue-Tek O.C.T. (Sakura Finetek) and stored at -80°C. The remainder of the liver was fixed in 10% neutral buffered formalin. Tissues were processed, paraffin embedded, cut into 4–5 μ sections and stained with hematoxylin and eosin. Additional liver sections were stained with Oil Red-O or pico- Sirius Red. Tissues were evaluated by a pathologist blinded to sample identity and study design. Hepatic fat accumulation, inflammation and fibrosis were scored on an ascending 0–4 scale.[49]

Quantitative PCR. RNA was extracted from liver samples using the E.Z.N.A Total RNA Kit (Omega), and residual genomic DNA was removed with DNase treatment (Omega), using the manufacturer's recommendations. Total RNA (1–2 μg) was used for synthesis of complimentary DNA (qScript cDNA Synthesis Kit; Quanta Biosciences). PerfeCTa SYBR Green FastMix, Low ROX quantitative polymerase chain reaction (PCR) Master Mix (Quanta Biosciences) was used for the quantitative PCR reaction utilizing Applied Biosystems 7500. Gene expression levels were normalized to *Gapdh* expression, and quantification was determined via the $\Delta\Delta C_T$ method using the *Atm*$^+$ SD group as the comparative delta value (expression of 1). Error bars represent relative log conversion of standard error as described previously in reference 50. Primer sets were acquired (Integrated DNA Technologies) as follows: glyceraldehyde-3-phosphate dehydrogenase (Gapdh), p22phox, Puma, Fas and Fas Receptor (**Table S1**).

Immunohistochemistry. Hepatocyte apoptosis was quantified by terminal deoxynucleotidyl transferase-mediated deoxyuridine triphosphate nick-end labeling per manufacturers recommendation (TUNEL; ApopTag Peroxidase In Situ Apoptosis Detection Kit; Millipore). Positive staining was detected with 3,3'-diaminobenzidine tetrahydrochloride (DAB) (Invitrogen) and sections were counterstained with hematoxylin. Liver sections from 5 animals per group were TUNEL stained. For each section, four 20x fields were chosen randomly and the number of TUNEL-positive and TUNEL-negative hepatocytes were quantified.

Immunohistologic detection of phosphorylated H2AX was determined on formalin-fixed, paraffin embedded liver sections. Briefly, sections were deparaffinized and rehydrated. Antigen retrieval was performed by heating the samples to 95°C in 0.25 mM EDTA, pH 8, over 50 min. Sections were treated with 3% H_2O_2 for 10 min and blocked with 4% bovine serum albumin and 20% Tween in 1x TBS at room temperature and then incubated overnight with primary antibody (1:200 dilution; mouse monoclonal anti-γH2AX antibody; Millipore) at 4°C. Slides were treated with biotinylated secondary antibody for 20 min and detected with Histostain Kit (Invitrogen). Quantification of positive γH2AX hepatocytes was performed in the same manner described for TUNEL staining.

Hydrogen peroxide, 8-hydroxyguanosine, phospho-ATM and dihydrorhodamine imaging and quantification. Hepatic H_2O_2 levels were detected using the Amplex Red Hydrogen Peroxide/Peroxidase Assay Kit (Molecular Probes). Single-cell hepatocyte suspensions were obtained from fresh liver samples, and red blood cells were removed using a percol gradient. Reactions containing 50 μM Amplex Red reagent, 0.1 U/mL horse radish peroxidase and 1 x 10^5 hepatocytes in 50 mM sodium phosphate buffer, pH 7.4, were incubated for 30 min at 37°C. Fluorescence was measured with a microplate reader using excitation at 530 nm and fluorescence detection at 590 nm. Absolute H_2O_2 levels were determined in relationship to a standard curve.

Hepatic superoxide was visualized using dihydrorhodamine 123 (DHR) (Molecular Probes/Invitrogen) fluorescent imaging. Hepatocytes were harvested similarly to the H_2O_2 assay. Hepatocytes were washed in 1x PBS, resuspended in media and incubated with 100 μL of 25 μg/mL solution of DHR in the dark at 37°C for 20 min. Hepatocytes were counted, and cytospins were performed with 1 x 10^6 cells. Images were obtained via confocal microscopy using excitation 596 nm, detection at 600–650 nm and magnification 63x.[51] Nuclei were stained with 4',6-diamidino-2-phenylindole (DAPI) (Sigma-Aldrich). Mean red fluorescent values were determined by averaging the fluorescence within a set number of pixels placed over five areas within a 63x field, three fields per sample. Results were expressed on a scale of 0–250.

DNA damage in hepatocytes was detected using an anti-8-hydroxyguanosine (8-OHG) antibody (ab10802, Abcam), and the presence of phosphorylated ATM in hepatocytes was detected using an anti-phospho-Serine1981-ATM (p-ATM) antibody (#200-301-400, Rockland) on frozen liver sections. Liver samples were embedded in Tissue-Tek O.C.T., flash frozen in liquid N_2 and sectioned at 8–10 μM. Sections were fixed in a mixture of three parts acetone, one part pure ethanol and washed in 1x PBS. Sections were blocked with casein/10% donkey serum for 20 min at room temperature, washed in 1x PBS and then incubated with goat anti-8-OHG antibody (1:100 dilution) for 1 h at 37°C or mouse anti-p-ATM antibody (1:200 dilution) overnight at 4°C in a humidifying chamber. Sections were washed in 1x PBS and treated with secondary antibodies labeled with Texas Red (1:500 dilution; Jackson ImmunoResearch). Nuclei were labeled with 4',6-diamidino-2-phenylindole (DAPI) (Sigma-Aldrich). For 8-OHG quantification, the percentage of positive 8-OHG cells was calculated over three 80x fields from three different mice per group.

Western blotting. Cells were harvested and solubilized in RIPA buffer as described previously in reference 52, followed by sonication. Total protein was quantified by Bradford assay, resolved on 6% to 14% SDS-PAGE gels, and subjected to immunoblotting using antibodies against PUMA (Abcam, #ab9643) and anti-β-actin (Sigma, #A5441). Western blot imaging and quantification was performed using a Versa Doc Imaging System (Bio-Rad Laboratories).

Statistical analyses. Parametric data were analyzed utilizing one-way analysis of variance followed by Tukey's post-test or by t-test. Nonparametric data were analyzed by the

Mann-Whitney-U test followed by Dunn's post test. p-values of ≤ 0.05 were considered statistically significant. Data are presented as mean ± standard error of the mean unless otherwise specified. All analyses were made with GraphPad Prism version 5.0 for Windows (GraphPad Software).

Disclosure of Potential Conflicts of Interest

No potential conflicts of interest were disclosed.

Acknowledgments

The authors thank Eric Denkers and his lab for valuable suggestions and the use of substrates; Luce Guanzini for reading and editing the manuscript; and Drew Kirby for technical support.

This work was supported by the Cornell University College of Veterinary Medicine Dean's Fund for Clinical Excellence (to E.K.D.); the Cornell University College of Veterinary Medicine Clinical Fellowship Program (to E.K.D.); a Cornell University College of Veterinary Medicine Graduate Research Assistantship (to G.B.); and NIH grants R01 CA108773 (to R.S.W.), R03 HD058220 (to R.S.W.) and K08 DK077728 (to K.J.M.). Irradiations were performed with shared instrumentation supported by NCRR grant S10RR023781.

Note

Supplemental materials can be found at:
www.landesbioscience.com/journals/cc/article/20259

References

1. Cohen JC, Horton JD, Hobbs HH. Human fatty liver disease: old questions and new insights. Science 2011; 332:1519-23; PMID:21700865; http://dx.doi.org/10.1126/science.1204265.
2. Starley BQ, Calcagno CJ, Harrison SA. Nonalcoholic fatty liver disease and hepatocellular carcinoma: a weighty connection. Hepatology 2010; 51:1820-32; PMID:20432259; http://dx.doi.org/10.1002/hep.23594.
3. Williams CD, Stengel J, Asike MI, Torres DM, Shaw J, Contreras M, et al. Prevalence of nonalcoholic fatty liver disease and nonalcoholic steatohepatitis among a largely middle-aged population utilizing ultrasound and liver biopsy: a prospective study. Gastroenterology 2011; 140:124-31; PMID:20858492; http://dx.doi.org/10.1053/j.gastro.2010.09.038.
4. Hardwick RN, Fisher CD, Canet MJ, Lake AD, Cherrington NJ. Diversity in antioxidant response enzymes in progressive stages of human nonalcoholic fatty liver disease. Drug Metab Dispos 2010; 38:2293-301; PMID:20805291; http://dx.doi.org/10.1124/dmd.110.035006.
5. Caldwell S, Park SH. The epidemiology of hepatocellular cancer: from the perspectives of public health problem to tumor biology. J Gastroenterol 2009; 44:96-101; PMID:19148801; http://dx.doi.org/10.1007/s00535-008-2258-6.
6. Mehta K, Van Thiel DH, Shah N, Mobarhan S. Nonalcoholic fatty liver disease: pathogenesis and the role of antioxidants. Nutr Rev 2002; 60:289-93; PMID:12296456; http://dx.doi.org/10.1301/002966402320387224.
7. Ong J, Younossi ZM, Reddy V, Price LL, Gramlich T, Mayes J, et al. Cryptogenic cirrhosis and post-transplantation nonalcoholic fatty liver disease. Liver Transpl 2001; 7:797-801; PMID:11552214; http://dx.doi.org/10.1053/jlts.2001.24644.
8. Kusminski CM, Shetty S, Orci L, Unger RH, Scherer PE. Diabetes and apoptosis: lipotoxicity. Apoptosis 2009; 14:1484-95; PMID:19421860; http://dx.doi.org/10.1007/s10495-009-0352-8.
9. Cazanave SC, Elmi NA, Akazawa Y, Bronk SF, Mott JL, Gores GJ. CHOP and AP-1 cooperatively mediate PUMA expression during lipoapoptosis. Am J Physiol Gastrointest Liver Physiol 2010; 299:236-43; PMID:20430872; http://dx.doi.org/10.1152/ajpgi.00091.2010.
10. Feldstein A, Gores GJ. Steatohepatitis and apoptosis: therapeutic implications. Am J Gastroenterol 2004; 99:1718-9; PMID:15330908; http://dx.doi.org/10.1111/j.1572-0241.2004.40573.x.
11. Feldstein AE, Gores GJ. Apoptosis in alcoholic and nonalcoholic steatohepatitis. Front Biosci 2005; 10:3093-9; PMID:15970563; http://dx.doi.org/10.2741/1765.
12. Machado MV, Cortez-Pinto H. Cell death and nonalcoholic steatohepatitis: where is ballooning relevant? Expert Rev Gastroenterol Hepatol 2011; 5:213-22; PMID:21476916; http://dx.doi.org/10.1586/egh.11.16.
13. Noguchi Y, Young JD, Aleman JO, Hansen ME, Kelleher JK, Stephanopoulos G. Tracking cellular metabolomics in lipoapoptosis- and steatosis-developing liver cells. Mol Biosyst 2011; 7:1409-19; PMID:21327189; http://dx.doi.org/10.1039/c0mb00309c.
14. Sunny NE, Parks EJ, Browning JD, Burgess SC. Excessive hepatic mitochondrial TCA cycle and gluconeogenesis in humans with nonalcoholic fatty liver disease. Cell Metab 2011; 14:804-10; PMID:22152305; http://dx.doi.org/10.1016/j.cmet.2011.11.004.
15. McKinnon PJ. ATM and the molecular pathogenesis of ataxia telangiectasia. Annu Rev Pathol 2012; 7:303-21; PMID:22035194; http://dx.doi.org/10.1146/annurev-pathol-011811-132509.
16. Armata HL, Golebiowski D, Jung DY, Ko HJ, Kim JK, Sluss HK. Requirement of the ATM/p53 tumor suppressor pathway for glucose homeostasis. Mol Cell Biol 2010; 30:5787-94; PMID:20956556; http://dx.doi.org/10.1128/MCB.00347-10.
17. Ditch S, Paull TT. The ATM protein kinase and cellular redox signaling: beyond the DNA damage response. Trends Biochem Sci 2012; 37:15-22; PMID:22079189; http://dx.doi.org/10.1016/j.tibs.2011.10.002.
18. Guo Z, Kozlov S, Lavin MF, Person MD, Paull TT. ATM activation by oxidative stress. Science 2010; 330:517-21; PMID:20966255; http://dx.doi.org/10.1126/science.1192912.
19. Barzilai A, Yamamoto K. DNA damage responses to oxidative stress. DNA Repair (Amst) 2004; 3:1109-15; PMID:15279799; http://dx.doi.org/10.1016/j.dnarep.2004.03.002.
20. Gao D, Wei C, Chen L, Huang J, Yang S, Diehl AM. Oxidative DNA damage and DNA repair enzyme expression are inversely related in murine models of fatty liver disease. Am J Physiol Gastrointest Liver Physiol 2004; 287:1070-7; PMID:15231485; http://dx.doi.org/10.1152/ajpgi.00228.2004.
21. Matsuzawa N, Takamura T, Kurita S, Misu H, Ota T, Ando H, et al. Lipid-induced oxidative stress causes steatohepatitis in mice fed an atherogenic diet. Hepatology 2007; 46:1392-403; PMID:17929294; http://dx.doi.org/10.1002/hep.21874.
22. Barzilai A, Rotman G, Shiloh Y. ATM deficiency and oxidative stress: a new dimension of defective response to DNA damage. DNA Repair (Amst) 2002; 1:3-25; PMID:12509294; http://dx.doi.org/10.1016/S1568-7864(01)00007-6.
23. Bakkenist CJ, Kastan MB. DNA damage activates ATM through intermolecular autophosphorylation and dimer dissociation. Nature 2003; 421:499-506; PMID:12556884; http://dx.doi.org/10.1038/nature01368.
24. Barlow C, Hirotsune S, Paylor R, Liyanage M, Eckhaus M, Collins F, et al. Atm-deficient mice: a paradigm of ataxia telangiectasia. Cell 1996; 86:159-71; PMID:8689683; http://dx.doi.org/10.1016/S0092-8674(00)80086-0.
25. Elson A, Wang Y, Daugherty CJ, Morton CC, Zhou F, Campos-Torres J, et al. Pleiotropic defects in ataxia-telangiectasia protein-deficient mice. Proc Natl Acad Sci USA 1996; 93:13084-9; PMID:8917548; http://dx.doi.org/10.1073/pnas.93.23.13084.
26. Xu Y, Ashley T, Brainerd EE, Bronson RT, Meyn MS, Baltimore D. Targeted disruption of ATM leads to growth retardation, chromosomal fragmentation during meiosis, immune defects and thymic lymphoma. Genes Dev 1996; 10:2411-22; PMID:8843194; http://dx.doi.org/10.1101/gad.10.19.2411.
27. Kinner A, Wu W, Staudt C, Iliakis G. Gamma-H2AX in recognition and signaling of DNA double-strand breaks in the context of chromatin. Nucleic Acids Res 2008; 36:5678-94; PMID:18772227; http://dx.doi.org/10.1093/nar/gkn550.
28. Yu J, Zhang L. PUMA, a potent killer with or without p53. Oncogene 2008; 27:71-83; PMID:19641508; http://dx.doi.org/10.1038/onc.2009.45.
29. Krizhanovsky V, Yon M, Dickins RA, Hearn S, Simon J, Miething C, et al. Senescence of activated stellate cells limits liver fibrosis. Cell 2008; 134:657-67; PMID:18724938; http://dx.doi.org/10.1016/j.cell.2008.06.049.
30. Povero D, Busletta C, Novo E, di Bonzo LV, Cannito S, Paternostro C, et al. Liver fibrosis: a dynamic and potentially reversible process. Histol Histopathol 2010; 25:1075-91; PMID:20552556.
31. Zhan SS, Jiang JX, Wu J, Halsted C, Friedman SL, Zern MA, et al. Phagocytosis of apoptotic bodies by hepatic stellate cells induces NADPH oxidase and is associated with liver fibrosis in vivo. Hepatology 2006; 43:435-43; PMID:16496318; http://dx.doi.org/10.1002/hep.21093.
32. Canbay A, Friedman S, Gores GJ. Apoptosis: the nexus of liver injury and fibrosis. Hepatology 2004; 39:273-8; PMID:14767974; http://dx.doi.org/10.1002/hep.20051.
33. Villunger A, Michalak EM, Coultas L, Müllauer F, Böck G, Ausserlechner MJ, et al. p53- and drug-induced apoptotic responses mediated by BH3-only proteins puma and noxa. Science 2003; 302:1036-8; PMID:14500851; http://dx.doi.org/10.1126/science.1090072.
34. Cazanave SC, Mott JL, Elmi NA, Bronk SF, Werneburg NW, Akazawa Y, et al. JNK1-dependent PUMA expression contributes to hepatocyte lipoapoptosis. J Biol Chem 2009; 284:26591-602; PMID:19638343; http://dx.doi.org/10.1074/jbc.M109.022491.
35. Michalak EM, Jansen ES, Happo L, Cragg MS, Tai L, Smyth GK, et al. Puma and to a lesser extent Noxa are suppressors of Myc-induced lymphomagenesis. Cell Death Differ 2009; 16:684-96; PMID:19148184; http://dx.doi.org/10.1038/cdd.2008.195.

36. Michalak EM, Villunger A, Adams JM, Strasser A. In several cell types tumour suppressor p53 induces apoptosis largely via Puma but Noxa can contribute. Cell Death Differ 2008; 15:1019-29; PMID:18259198; http://dx.doi.org/10.1038/cdd.2008.16.
37. Farinati F, Cardin R, Bortolami M, Grottola A, Manno M, Colantoni A, et al. Estrogens receptors and oxidative damage in the liver. Mol Cell Endocrinol 2002; 193:85-8; PMID:12161006; http://dx.doi.org/10.1016/S0303-7207(02)00100-4.
38. Lu S, Shen KC, Wang Y, Brooks SC, Wang YA. Impaired hepatocyte survival and liver regeneration in Atm-deficient mice. Hum Mol Genet 2005; 14:3019-25; PMID:16141284; http://dx.doi.org/10.1093/hmg/ddi333.
39. Nunomura A, Perry G, Pappolla MA, Wade R, Hirai K, Chiba S, et al. RNA oxidation is a prominent feature of vulnerable neurons in Alzheimer's disease. J Neurosci 1999; 19:1959-64; PMID:10066249.
40. Woodbine L, Brunton H, Goodarzi AA, Shibata A, Jeggo PA. Endogenously induced DNA double strand breaks arise in heterochromatic DNA regions and require ataxia telangiectasia mutated and Artemis for their repair. Nucleic Acids Res 2011; 39:6986-97; PMID:21596788; http://dx.doi.org/10.1093/nar/gkr331.
41. El-Serag HB. Hepatocellular carcinoma. N Engl J Med 2011; 365:1118-27; PMID:21992124; http://dx.doi.org/10.1056/NEJMra1001683.
42. Yasui K, Hashimoto E, Komorizono Y, Koike K, Arii S, Imai Y, et al.; Japan NASH Study Group, Ministry of Health, Labour and Welfare of Japan. Characteristics of patients with nonalcoholic steatohepatitis who develop hepatocellular carcinoma. Clin Gastroenterol Hepatol 2011; 9:428-33; PMID:21320639; http://dx.doi.org/10.1016/j.cgh.2011.01.023.
43. Tang D, Lotze MT, Kang R, Zeh HJ. Apoptosis promotes early tumorigenesis. Oncogene 2011; 30:1851-4; PMID:21151175; http://dx.doi.org/10.1038/onc.2010.573.
44. Dowman JK, Armstrong MJ, Tomlinson JW, Newsome PN. Current therapeutic strategies in non-alcoholic fatty liver disease. Diabetes Obes Metab 2011; 13:692-702; PMID:21449949; http://dx.doi.org/10.1111/j.1463-326.2011.01403.x.
45. Foster T, Budoff MJ, Saab S, Ahmadi N, Gordon C, Guerci AD. Atorvastatin and antioxidants for the treatment of nonalcoholic fatty liver disease: the St. Francis Heart Study randomized clinical trial. Am J Gastroenterol 2011; 106:71-7; PMID:20842109; http://dx.doi.org/10.1038/ajg.2010.299.
46. Reliene R, Schiestl RH. Antioxidants suppress lymphoma and increase longevity in Atm-deficient mice. J Nutr 2007; 137:229-32; PMID:17182831.
47. Reliene R, Schiestl RH. Experimental antioxidant therapy in ataxia telangiectasia. Clin Med Oncol 2008; 2:431-6; PMID:21892312.
48. Schubert R, Erker L, Barlow C, Yakushiji H, Larson D, Russo A, et al. Cancer chemoprevention by the antioxidant tempol in Atm-deficient mice. Hum Mol Genet 2004; 13:1793-802; PMID:15213104; http://dx.doi.org/10.1093/hmg/ddh189.
49. Rogers AB, Boutin SR, Whary MT, Sundina N, Ge Z, Cormier K, et al. Progression of chronic hepatitis and preneoplasia in *Helicobacter hepaticus*-infected A/JCr mice. Toxicol Pathol 2004; 32:668-77; PMID:15513910; http://dx.doi.org/10.1080/01926230490524247.
50. Maurer KJ, Rao VP, Ge Z, Rogers AB, Oura TJ, Carey MC, et al. T-cell function is critical for murine cholesterol gallstone formation. Gastroenterology 2007; 133:1304-15; PMID:17919501; http://dx.doi.org/10.1053/j.gastro.2007.07.005.
51. Sobreira C, Davidson M, King MP, Miranda AF. Dihydrorhodamine 123 identifies impaired mitochondrial respiratory chain function in cultured cells harboring mitochondrial DNA mutations. J Histochem Cytochem 1996; 44:571-9; PMID:8666742; http://dx.doi.org/10.1177/44.6.8666742.
52. Harlow E, Lane D. Lysing Tissue-Culture Cells for Immunoprecipitation. Cold Spring Harbor Protocols 2006; 2006:4531; http://dx.doi.org/10.1101/pdb.prot4531.